Wind and Structures, *Vol. 21, No. 6 (2015) 657-675*
DOI: http://dx.doi.org/10.12989/was.2015.21.6.657

Numerical evaluation for vibration-based damage detection in wind turbine tower structure

Tuan-Cuong Nguyen[a], Thanh-Canh Huynh[b] and Jeong-Tae Kim[*]

Department of Ocean Engineering, Pukyong National University, 45 Yongso-ro, Nam-gu, Busan, Korea

(Received November 15, 2014, Revised October 1, 2015, Accepted December 2, 2015)

Abstract. In this study, the feasibility of vibration-based damage detection methods for the wind turbine tower (WTT) structure is evaluated. First, a frequency-based damage detection (FBDD) is outlined. A damage-localization algorithm is visited to locate damage from changes in natural frequencies. Second, a mode-shape-based damage detection (MBDD) method is outlined. A damage index algorithm is utilized to localize damage from estimating changes in modal strain energies. Third, a finite element (FE) model based on a real WTT is established by using commercial software, Midas FEA. Several damage scenarios are numerically simulated in the FE model of the WTT. Finally, both FBDD and MBDD methods are employed to identify the damage scenarios simulated in the WTT. Damage regions are chosen close to the bolt connection of WTT segments; from there, the stiffness of damage elements are reduced.

Keywords: frequency-based damage detection, mode-shape-based damage detection, wind turbine tower structure, Midas FEA

1. Introduction

In recent years, wind energy has been considered as a well-known renewable energy source. To harvest more energy, basically, the wind turbine is needed to be larger. Accordingly, the tower and blade of the wind turbine structure should be increased in height and length. Associated with the great development of wind turbine project, however, a lot of corresponding problems should be dealt in order to prevent the occurrence of unfortunate accidents. In most cases, steel wind turbine structures are pre-fabricated in factories and assembled in the field via in-situ structural joints. During the construction and operation of the wind turbine, damage can occur in any components or parts of the structure, which include blades, steel tower segments, and concrete foundation.

In the past few decades, the nondestructive damage identification has gained increasing attentions from the scientific and engineering communities. More specifically, structural health monitoring based on vibration responses has received much more concerns since it offers several important advantages as compared to other techniques. The advantages are as follows: (1) the time period required to perform vibrational measurements can be short; (2) damage detection is not

∗Corresponding author, Professor, E-mail: idis@pknu.ac.kr
[a] Graduate Student, E-mail: ce.cuongnt@gmail.com
[b] Graduate Student, E-mail: ce.huynh@gmail.com

http://www.techno-press.org/?journal=was&subpage=8 ISSN: 1226-6116 (Print), 1598-6225 (Online)

restricted to a local area; (3) damage could be alarmed and located by measuring only changes in natural frequencies, which can be easily obtained from vibration signals of a single acquisition point. Many studies have been performed for damage monitoring of civil structures utilizing changes in dynamic characteristics (Doebling *et al.* 1998, Shi *et al.* 1998, Brownjohn *et al*. 2001, Catbas *et al.* 2008, Jang *et al.* 2010). Also, research attempts have been made for developing damage detection algorithms such as modal sensitivity method, modal flexibility method, genetic algorithm, neural network and so on (Kim and Stubbs 1995, Atkan *et al*. 1997, Levin and Lieven 1998, Yun and Bahng 2000, Yun *et al.* 2009).

Up-to-date, many local nondestructive monitoring methods are utilized for damage detection in WTT structures, not only in lab-scale models but also in field experiment tests, such as: acoustic emission method (Sutherland *et al*. 1994, Joosse *et al*. 2002), thermal imaging method (Dutton 2004, Hahn *et al.* 2002), fiber optics techniques (Lee and Tsuda 2005, Perez *et al*. 2001), laser Doppler vibrometer method (Ghoshal *et al.* 2000), electrical resistance-based method (Matsuzaki and Todoroki 2006). However, only a few studies have been made for structural condition monitoring of WTT structures using vibration measurement (Swartz *et al*. 2010, Devriendt *et al.* 2014).

Damage-induced changes in structural parameters, such as reduction in stiffness or loosening of connection, will cause detectable changes in the modal properties (Farrar *et al*. 1997, Gross *et al.* 1999, Zhang *et al.* 1999, Ciang *et al.* 2008). As compared to other modal parameters, natural frequency is relatively convenient to utilize for identifying damage locations. The most appealing feature associated with using the natural frequency is that they are relatively simple to measure. However, the feasibility of using the natural frequency for the purpose of damage localization is limited for at least three reasons. Firstly, even a significant damage may cause very small changes in natural frequencies, particularly for larger structures. Secondly, these changes may go undetected due to measurement or processing errors (Kim and Stubbs 2003). Thirdly, ambient temperature variation may cause thermal-induced variation of modal properties (Kim *et al.* 2004).

The objective of the paper is to evaluate the feasibility of vibration-based damage detection methods for WTT structures. First, a frequency-based damage detection (FBDD) method is outlined. An frequency-based algorithm is formulated to locate damage from changes in natural frequencies. Second, a mode-shape-based damage detection (MBDD) method is outlined. A mode-shape-based algorithm is formulated to localize damage from estimating changes in modal strain energies. Third, a finite element (FE) model based on a real WTT is established by using commercial software, Midas FEA. Several damage scenarios are numerically simulated in the FE model of the WTT. Finally, both FBDD and MBDD methods are employed to identify the damage scenarios simulated in the WTT. Damage regions are chosen close to the bolt connection of the WTT segments.

2. Vibration-based damage detection method

For a MDOF structural system with NE elements (j = 1, 2, 3, …, q, …, NE), the damage inflicted at predefined locations can be predicted by using modal information of NM vibration modes (i = 1, 2, 3, …, m, n, …, NM). Consequently, the i^{th} natural frequency ω_i and the i^{th} mode shape ϕ_i of an undamaged MDOF structural system are determined from the characteristic equation. Assume that at some later time the structure is damaged in one or more locations. The resulting characteristic equation of the damaged structure yields the modal parameters ω_i^* and ϕ_i^*.

Note that the asterisk represents for the damaged state.

2.1 Frequency-based Damage Detection (FBDD) method (Kim et al. 2003)

In term of natural frequency approach, a sensitivity equation is given to predict the damage at predefined locations of a MDOF structural system with NE elements and N nodes as follows

$$\sum_{j=1}^{NE} F_{ij}\alpha_j = Z_i \tag{1}$$

where α_j ($-1 \le \alpha_j \le 0$) is the damage inflicted at the j^{th} location, i.e., the fractional reduction in the j^{th} element's stiffness parameter. The term F_{ij} is the fractional changes of modal strain energy of the j^{th} element that is calculated for the i^{th} mode and is given by

$$F_{ij} = \frac{\{\phi_i\}^T \left[C_j\right]\{\phi_i\}}{\{\phi_i\}^T \left[C\right]\{\phi_i\}} \tag{2}$$

in which $[C_j]$ is the j^{th} stiffness matrix and $[C]$ is the system stiffness matrix.

The term Z_i is the fractional change in the i^{th} eigenvalue due to the damage, if changes in mass are neglected, then it is given by

$$Z_i = \delta\omega_i^2 / \omega_i^2 = \left(\omega_i^{*2} - \omega_i^2\right) / \omega_i^2 \tag{3}$$

By considering for all NM modes, the relation between the ratio of the fractional change in eigenvalues and the ratio of the modal strain energy can be formulated

$$Z_i \Big/ \sum_{k=1}^{NM} Z_k = F_{ij} \Big/ \sum_{k=1}^{NM} F_{kj} \tag{4}$$

Note that Eq. (4) is true only if the j^{th} element is damaged. Thus, an error index is introduced in Eq. (4) as follows

$$e_{ij} = Z_i \Big/ \sum_{k=1}^{NM} Z_k - F_{ij} \Big/ \sum_{k=1}^{NM} F_{kj} \tag{5}$$

where e_{ij} represents localization error for the i^{th} mode and the j^{th} location, and $e_{ij} = 0$ indicates that the damage is located at the j^{th} location using the i^{th} modal information. To account for all available modes, a single damage indicator (DI) of the j^{th} member is defined as

$$DI_j = \left[\sum_{i=1}^{NM} e_{ij}^2\right]^{-1/2} \tag{6}$$

where $0 \le DI_j < \infty$. Hence, the damage is located at the j^{th} element if DI_j approaches the local maximum point.

2.2 Mode-shape-based Damage Detection (MBDD) method (Kim et al. 2003)

In term of mode shape approach, a MDOF structural system with NE elements and N nodes is consider. Assume that the input-output relation of the structure is linear. Also assume a solution of the associated dynamic eigenvalue problem, then the ith modal stiffness, K_i, of the beam is calculated by

$$K_i = \int_0^L k(x)[\phi_i^{''}(\mathrm{x})]^2 dx \tag{7}$$

where $\phi_i(x)$ is the mode shape of the ith modal vector and k(x) is the bending stiffness of the beam (i.e., the product of Young's modulus and the second moment of area). The contribution of the jth element to the ith modal stiffness, K_{ij}, is given by

$$K_{ij} = k_j \int_j [\phi_i^{''}(\mathrm{x})]^2 dx \tag{8}$$

where k_j is the stiffness of the jth element and the integral is over the jth element's length. Then, the fraction of modal energy (i.e., the undamaged modal sensitivity) of the ith mode and the jth element is defined as

$$F_{ij} = K_{ij} / K_i \tag{9}$$

By the similar analysis, the fraction of modal energy for the damaged structure can be formed as

$$F_{ij}^* = K_{ij}^* / K_i^* \tag{10}$$

in which these parameters K_{ij}^* and K_i^* are given by

$$K_{ij}^* = k_j^* \int_j [\phi_i^{''*}(\mathrm{x})]^2 dx \tag{11}$$

and

$$K_i^* = \int_0^L k^*(x)[\phi_i^{''*}(\mathrm{x})]^2 dx \tag{12}$$

Suppose that the factional modal sensitivities of the ith mode and the jth element of undamaged and damaged structure are approximately same ($F_{ij}^* \approx F_{ij}$). Then, the following expression is obtained

$$F_{ij}^* \big/ F_{ij} = \left(K_{ij}^* K_i\right) \big/ \left(K_{ij} K_i^*\right) = 1 \tag{13}$$

By substituting Eqs. (8) and (11) into Eq. (12) and by rearranging, a damage localization index for the jth location and the ith mode is defined as

$$\beta_{ij} = \frac{k_j}{k_j^*} = \frac{\gamma_{ij}^* K_i}{\gamma_{ij} K_i^*} = \frac{\gamma_{ij}^* \omega_i^2}{\gamma_{ij} \omega_i^{*2}} \tag{14}$$

where $\gamma_{ij} = \int_j [\phi_i^{''}(x)]^2 dx$ and $\gamma_{ij}^* = \int_j [\phi_i^{''*}(x)]^2 dx$. To apply for all NM vibration modes, a damage localization index for the j[th] location is formulated

$$\beta_j = \sum_{i=1}^{NM} Num \Big/ \sum_{i=1}^{NM} Den = \sum_{i=1}^{NM} \gamma_{ij}^* K_i \Big/ \sum_{i=1}^{NM} \gamma_{ij} K_i^* \tag{15}$$

where damage is indicated at the j[th] location if $\beta_j > 1$. By treating β_j as the random variable of NE samples, the damage j[th] location can be identified from the statistical pattern analysis.

3. Numerical evaluation on FE model of WTT

3.1 Description of test structure

Nowadays, the commercial wind turbine is mostly horizontal-axis-type with typically three blades, as illustrated in Fig. 1(a). The main subsystems of a horizontal axis wind turbine can be separated into 5 components: rotor, nacelle, tower, foundation and electrical system, as schematized in Fig. 1(b). The rotor includes the blades and the hub while the nacelle consists of gearbox, drive train, control parts and yaw system. The tower structure and the foundation are designed dependently on the types of turbine and onshore or offshore location. The balance of the electrical system contains cables, switchgear, transformers, and possibly electronic power converters.

In this study, a real WTT structure was selected to evaluate the feasibility of the FBDD method and the MBDD method. The target structure was 3 mega-watt onshore WTT located at Woljeong-ri, Jeju Island, Korea. The real WTT structure is 77 m in height consisting of 3 segments (see Fig. 2(a)) connected by preloaded bolted joints (see Fig. 2(b)). The first segment is 19 m in length while two other ones are 29 m in length (see Fig. 3(a)). Each segment is combined by several various cross-section conical sections which are bonded by using butt weld. Table 1 lists the section's thickness changes with respect to the increasing height. The outer diameters at the bottom and the top levels were 4.15 m and 2.3 m, respectively.

3.2 FE modeling

A FE model of the real WTT was established by using a commercial software, Midas FEA. In the FE modelling, the tower was simulated by shell elements with 10 different cross-section parts corresponding to the changes in the thickness, as shown in Fig. 3(a). The element size in vertical direction was chosen in such a way that almost square grid occurs. The same discretization with 36 quadrilateral elements in the circumferential direction was applied throughout the tower to ensure the consistency of mesh. The bolted ring flange joints were modeled as shell elements, in which the shell thicknesses were chosen close to the actual ones in the target structure. Note that the bolted joints could be seen as the most important locations in the WTT structure. As the preliminary study, the entrance gate and the blades were not simulated in the FE model. The mass of the rotor blades, the rotor and the nacelle were simplified as concentrated masses. According to technical data of the target WTT structure, the total mass of the rotor and the nacelle was approximately 107.8 tons which was simply assigned to a rigid node at the nacelle's level. The eccentricity of the rigid node was 1.88 m along the X direction. Ideally, the center of gravity of rotor-nacelle-assembly is mostly coincide with the center of a tower section to eliminate additional moment due to the eccentricity. However, there is inevitable eccentricity in real cases and it makes difference between the natural frequencies in fore-aft and side-side directions. We considered the eccentricity for numerical simulation to analyze the difference in mode shapes and natural frequencies.

(a) Onshore WTT

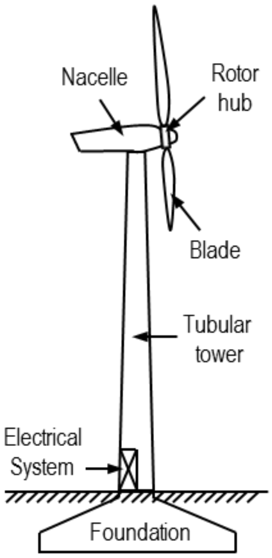

(b) Schematic of WTT

Fig. 1 A typical horizontal-axis-type WTT: target structure

(a) WTT segment

(b) Bolted ring flange

Fig. 2 A typical WTT connection of target structure

The FE model was meshed into 770 block elements along to the symmetric axis of the tower with 0.1 m intervals in height. The connection between the tower and the base was assumed as fixed end. The vibration of the rotor blades were simply neglected in the numerical simulation. Material properties of FE model were defined for steel elements with the elastic modulus E = 210 GPa, Poisson's ratio ν = 0.3 and the mass density ρ = 7850 kg/m^3.

The pre-damage and post-damage modal parameters of the FE model were numerically generated for Midas FEA. Hence, five damage scenarios were performed in which the damage locations were chosen close to the bolted ring flange (see Fig. 3(a)). In the real wind turbines, the damages are mostly observed near the connections between tower segments or between tower segment and concrete foundation as forms of concrete cracks and grouting failure.

The damage was simulated by reducing elastic modulus E to change the flexural rigidity EI because of assuming no change in structural mass due to damage. The mode shape vectors were acquired at 11 locations that are equally spaced along to symmetric axis of the tower as depicted in Fig. 3(b) (i.e., a sensor in every 7.7 m between two adjacent locations). The natural frequencies for the undamaged state and five damaged cases are listed in Table 2. The first three bending mode shapes of the undamaged structure are plotted in X direction and Y direction, as shown in Fig. 4. It is noted that those two sets are a little difference in their shapes and natural frequencies. In this study, we decided to utilize the X-directional mode shapes and natural frequencies for the damage detection process. Also, the pre-damage X-directional mode shapes were compared to the post-damage ones as shown in Fig. 5. It is clear that the amplitude changes in mode shapes could not be distinguished by the visual observation.

Table 1 Variation of cross-sectional thickness of WTT height

Height (m)	0 ÷ 5.4	5.4 ÷ 21.9	21.9 ÷ 30.6	30.6 ÷ 36.4	36.4 ÷ 42.2	42.2 ÷ 50.9	50.9 ÷ 53.8	53.8 ÷ 56.7	56.7 ÷ 59.6	59.6 ÷ 77
Thickness (mm)	40	26	24	23	22	21	19	18	17	16

Table 2 Damage scenarios and natural frequencies of WTT's FE model

Damage Case	Simulated Damage			X-directional Natural Freq. (Hz)		
	Damage Location		Severity (ΔEI/EI)	Mode 1	Mode 2	Mode 3
	Height (m)	Element				
Undamaged	-	-	-	0.3242	1.9402	4.1159
1	18.7	25	-0.25	0.3234	1.9388	4.1150
2	47.7	63	-0.25	0.3237	1.9380	4.1101
3	74.9	98	-0.25	0.3241	1.9338	4.0872
4	18.7, 47.7	25, 63	-0.25, -0.25	0.3230	1.9367	4.1093
5	18.7, 74.9	25, 98	-0.25, -0.25	0.3234	1.9325	4.0864

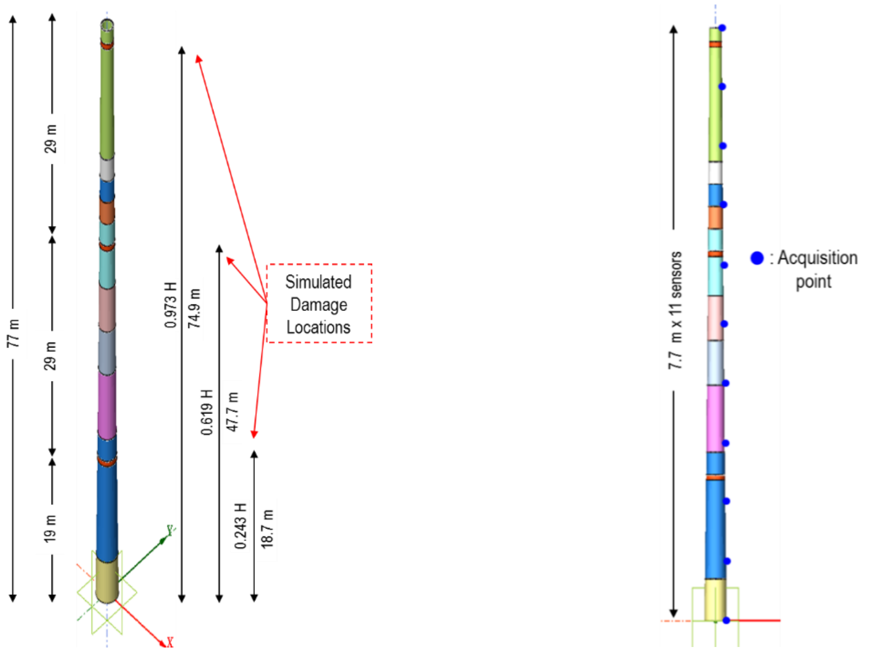

(a) Simulated damage locations (b) Data acquisition locations

Fig. 3 FE model of target WTT in Midas FEA

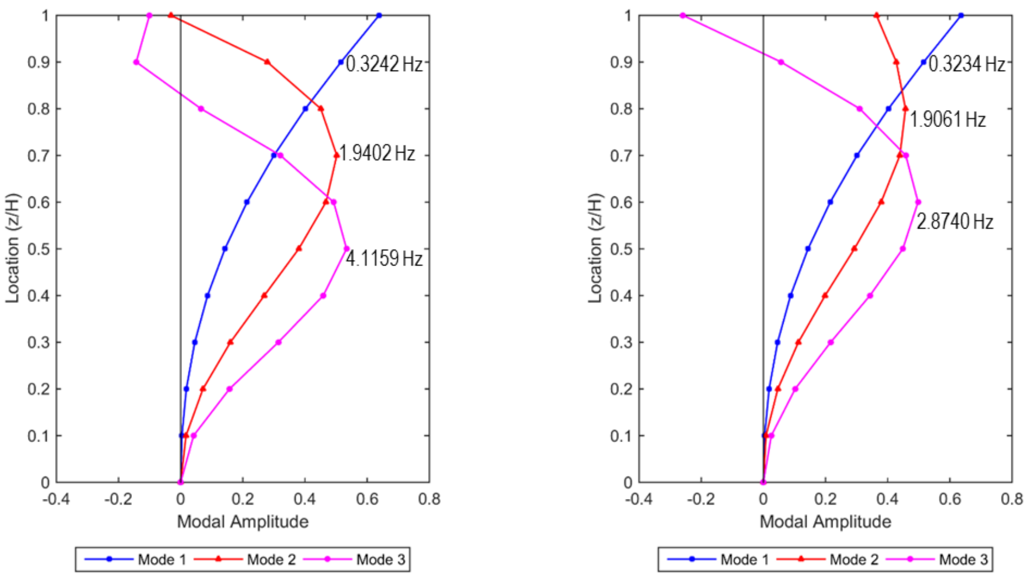

(a) X direction (b) Y direction

Fig. 4 First three bending mode shapes of WTT – undamaged case

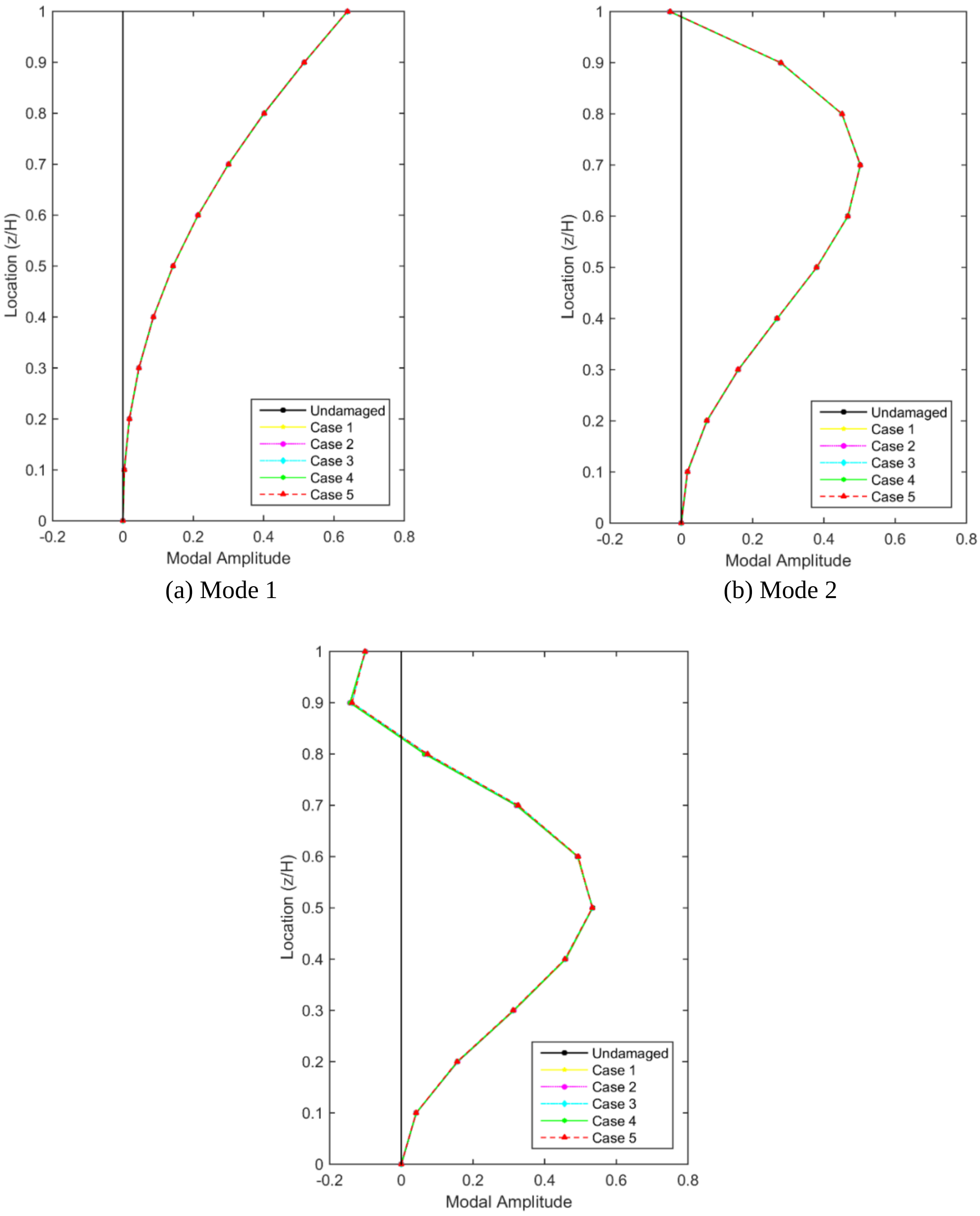

(a) Mode 1

(b) Mode 2

(c) Mode 3

Fig. 5 Comparison of x-directional mode shapes: undamaged vs damaged

3.3 Damage detection by FBDD method

The Euler–Bernoulli beam model was selected as the damage detection model (DDM). Modal parameters needed for the FBDD process (i.e., Eqs. (1)- (6)) are pre-damage, post-damage natural frequencies and pre-damage, post-damage mode shapes. The DDM of the structure consists of 100 beam elements with different size. Each DDM element is a potential damage location and has a spacing of 0.77 m or 1% of the beam span. We justify the use of a 0.77 m wide element by interpolating extracted modal vectors at the 101 nodal points of the damage detection model obtained by the use of spline functions and the element modal amplitude values from the mode shapes of the FE model. Using the interpolated modal coordinates for the beam, we generated functions $\phi(z)$, where z is the coordinate along the symmetric axis of the tower.

The modal sensitivity (corresponding to Eq. (2)) of i^{th} mode and j^{th} element between two locations (z_j, z_{j+1}) was computed by Kim *et al*. (2003)

$$F_{ij} = \int_{z_j}^{z_{j+1}} EI\left\{\phi_i''(\mathrm{z})\right\}^2 dz \Big/ K_i\,; K_i = \int_0^l EI\left\{\phi_i''(\mathrm{z})\right\}^2 dz \tag{16}$$

The curvatures of the mode shapes were generated at the 101 nodes of the DDM. Since three natural frequencies are available, the sensitivities are defined for 3 modes and 100 DDM elements. By using the Eq. (3), the factional changes in natural frequencies were computed by using the natural frequency data from Table 2. By assuming that the flexural rigidity EI is constant over the tower, the sensitivity ratio indicated by the right-hand side of Eq. (4) for an element q and for any two modes m and n can be rewritten by

$$\frac{F_{mq}}{F_{nq}} = \frac{\int_q \left\{\phi_m''(\mathrm{z})\right\}^2 dz}{\int_q \left\{\phi_n''(\mathrm{z})\right\}^2 dz} \cdot \frac{\int_0^l \left\{\phi_n''(\mathrm{z})\right\}^2 dz}{\int_0^l \left\{\phi_m''(\mathrm{z})\right\}^2 dz} \tag{17}$$

Next, localization errors were estimated using Eq. (5) for 3 modes and 100 locations by implementing the sensitivity ratios and the fractional changes in frequencies. The first term and the second term of Eq. (5) which represented for the error indices of the damage case 1 and damage case 4 are illustrated in Figs. 6 and 7. As shown in these figures, the change in frequency of the i^{th} mode was an invariant value, indicated by red line whereas the sensitivity ratios were variable corresponding to the j^{th} element, indicated by blue line. It should be noted that a potential damage location (PDL) was identified by the junction of the red line and the blue line, as marked by the black-down arrow plotted in Figs. 6 and 7.

Finally, the damage indices were computed to identify potential damage locations using Eq. (6). Note that the measurement noise was not considered in the numerical simulation and the modal parameter extraction. Therefore, to minimize the uncertainty errors caused by the measurement noise's effect or the computation errors, a decision-making rule based on the probability was utilized for assigning damage to a particular location. The values of the indicator was first normalized according to the rule

$$Z_j = \left(\beta_j - \mu_{\beta_j}\right) \Big/ \sigma_{\beta_j} \tag{18}$$

where $\mu_{\beta j}$ is the mean of β_j and $\sigma_{\beta j}$ is the standard deviation of β_j. The WTT elements were next assigned to a damage class via a statistical-pattern-recognition technique that utilizes hypothesis testing. The null hypothesis (i.e., H_0) was taken to be "the structure is undamaged at the j^{th} element" and the alternate hypothesis (i.e., H_1) was taken to be "the structure is damaged at the j^{th} element". In assigning damage to a particular location, the following decision rule were utilized: (1) choose H_1 if $Z_j \geq Z_0 = 1.5$ and (2) choose H_0 otherwise. A confidence level of 93% was used in the control chart.

Damage localization results by FBDD method are shown in Fig. 8 and listed in Table 3. For the damage case 1, the damage region was predicted as ranging from 16^{th} ~ 22^{th} DDM elements, see Fig. 8(a). The most probable damaged location was element 19 whereas the inflicted location was predefined at element 25. For the damage case 2, the predicted damage zone was only 64^{th} ~ 65^{th} DDM elements. The most potential damaged element was 65^{th} DDM element, which was well-matched to the inflicted location (i.e., 63^{th} DDM element), see Fig. 8(b). Although the FBDD method performed precisely to identify the simulated damage location, a false prediction can be observed near to the fixed end of WTT model, see Fig. 8(b). As noted in Fig. 7, the false alarming may be caused by the high sensitivities of all three modes near the fixed end. It is an inevitable error caused by choosing those three modes. An accurate damage detection result was obtained in the damage case 3, where the most probable predicted element exactly coincided with the inflicted element (i.e., DDM element 98), as shown in Fig. 8(c). As observed in Figs. 8(d) and 8(e), the FBDD method was seem to be underestimated to localize damage at two or more locations. For the damage cases 4 and 5, the FBDD method can predict only one of two simulated damage locations, heading to the free end of the WTT model.

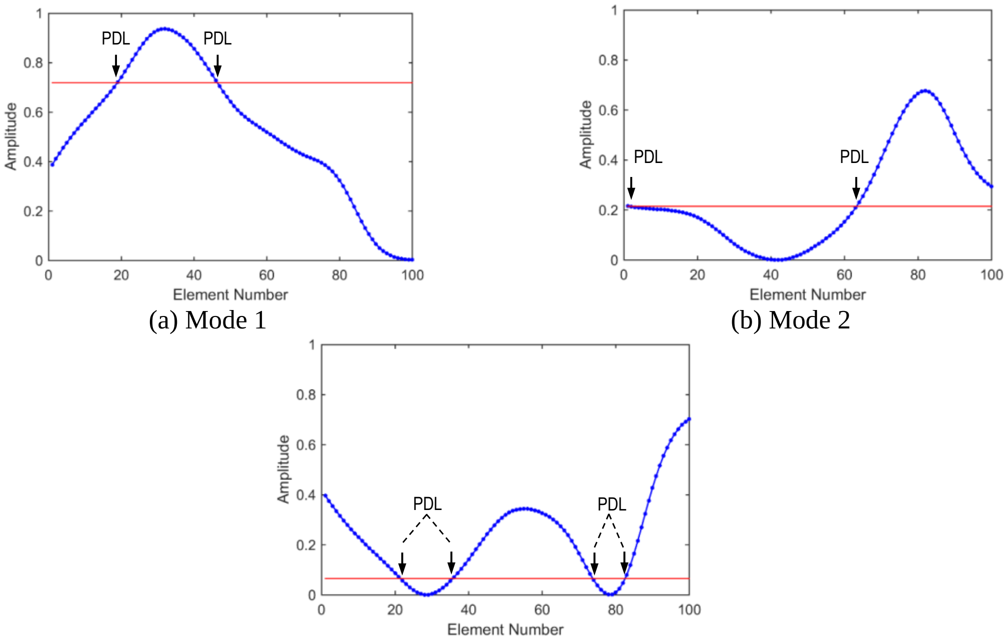

(a) Mode 1 (b) Mode 2

(c) Mode 3

Fig. 6 Modal sensitivity ratios and fractional changes of natural frequencies – damage case 1

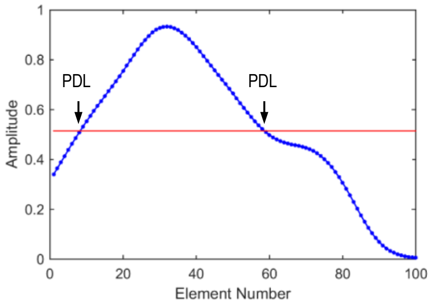

(a) Mode 1

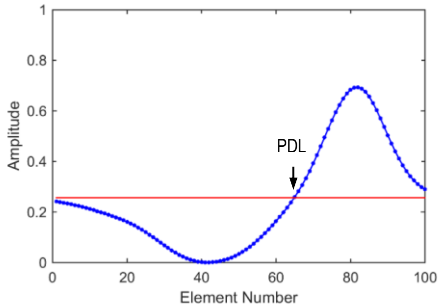

(b) Mode 2

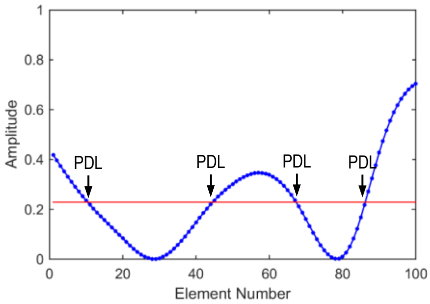

(c) Mode 3

Fig. 7 Modal sensitivity ratios and fractional changes of natural frequencies – damage case 4

Table 3 Damage prediction results of the WTT structure using FBDD method

Case	Inflicted Damage		Predicted Damage		Most Probable		Location Error
	Location	DDM	Location	Range of DDM	Location	DDM	(Δz/H) (%)
	z (m)	element	z (m)	element	z (m)	element	
1	18.7	25	11.9~16.6	16~22	14.2	19	5.84
2	47.7	63	48.9~49.6	64~65	49.6	65	2.47
3	74.9	98	74.3~76.6	97~100	74.9	98	0
4	18.7, 47.7	25, 63	5~8.1, 48.9~51.2	7~11, 64~67	6.5, 50.4	9, 66	15.84, 3.51
5	18.7, 74.9	25, 98	N/A, 68.9~76.6	N/A, 90~100	N/A, 72	N/A, 94	N/A, 3.77

The accuracy of the damage localization presented here was evaluated by measuring the so-called localization error le (Δz/H) × 100, in which Δz is the metrical difference between the inflicted damage location and the predicted location; and H is the WTT height. The localization errors of all damage cases are also listed in Table 3. For the single damage prediction, cases 1, 2 and 3, it was observed that the minimum localization error is 0% (damage case 3) and the maximum localization error is 5.84% (damage case 1). These results indicate that the predicted locations fell within 1.9 ~ 4.5 m of the correct locations in the test structure (H = 77 m as described in the previous section). For the multiple damage prediction, the localization errors of the detectable locations were 3.51% (damage case 4) and 3.77% (damage case 5) while those of undetectable ones were 15.84% (damage case 4) and N/A (damage case 5).

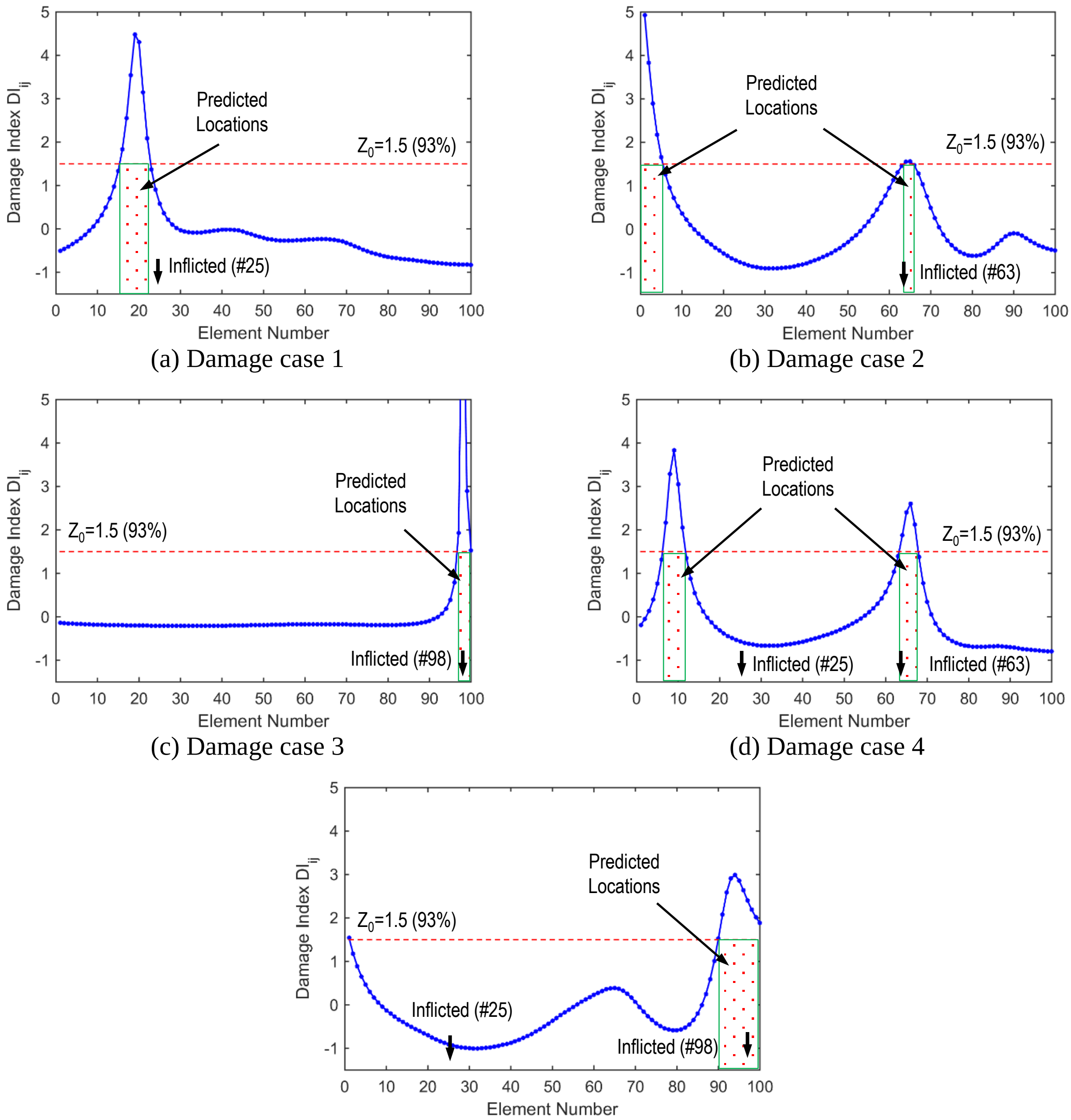

(a) Damage case 1 (b) Damage case 2

(c) Damage case 3 (d) Damage case 4

(e) Damage case 5

Fig. 8 Damage localization results by FBDD method

3.4 Damage detection by MBDD method

The Euler–Bernoulli beam model was selected as the DDM for MBDD method. As described in the previous section, the DDM of the structure consists of a total of 100 beam elements. Modal parameters needed for the MBDD process (i.e., Eqs. (7)-(15)) are pre-damage, post-damage natural frequencies and pre-damage, post-damage mode shapes. For individual mode shapes, pseudo reading at 101 nodal points of the damage detection model obtained via spline interpolation functions. Using the interpolated modal coordinates for each mode shape, the functions $\phi(z)$ and $\phi''(z)$ were generated, where z is the coordinate along the symmetric axis of the tower. The modal sensitivities of the undamaged case is shown in Fig. 9; and the comparisons of modal sensitivity before and after damage are shown in Fig. 10. As shown in Fig. 10, the changes in the modal sensitivities was clearly recognized for the first mode (see Fig. 10(a)), rather difficult for the second mode (see Fig. 10(b)), and almost impossible for the third mode (see Fig. 10(c)).

Next, the damage localization index of element j^{th} was computed for the five damage cases using Eq. (14). Then, by the same token, the MBDD indices were normalized according to the rule presented by Eq. (18). The damage localization results for the five damage cases are shown in Fig. 11 and listed in Table 4. The threshold was set at Z_o = 1.5 with the confidence level of 93%. For the damage case 1, the damage region was predicted as ranging from 19^{th} ~ 30^{th} DDM elements, see Fig. 11(a). However, the most probable damaged location was at DDM element 26, which was very close to the inflicted location (i.e., DDM element 25). For the damage case 2, the predicted damage zones were 26^{th} ~ 29^{th} and 57^{th} ~ 64^{th} DDM elements, see Fig. 11(b). Although the most potential damaged element was 61^{th} DDM element, which was rather matched to the inflicted location (i.e., 63^{th} DDM element), a false prediction can be observed heading to the fixed end of WTT model, see Fig. 11(b). For the damage case 3, no damage location was alarmed from the control chart, as shown in Fig. 11(c). The failure prediction was attributed to the insensitivity of mode shape curvature at free-end since the WTT was considered as a cantilever beam. A good damage location result was observed for the damage case 4, multiple damage. As observed in Fig. 11(d), the predicted locations were 24^{th} ~ 30^{th} and 59^{th} ~ 63^{th} DDM elements; and the most probable predicted elements (28^{th} and 61^{th} DDM elements) were well-matched with the inflicted elements (25^{th} and 63^{th} DDM elements). For the damage case 5, multiple damage, the MBDD method can predict only one of two simulated damage locations, which is close to the fixed end of the WTT model.

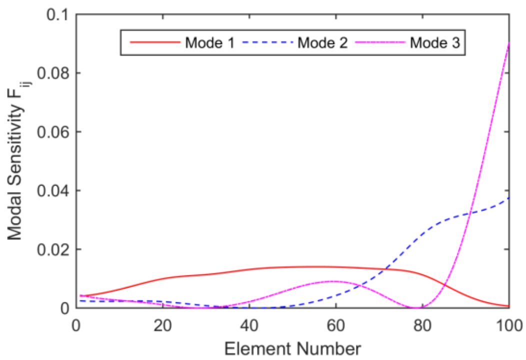

Fig. 9 Modal sensitivity of WTT structure – undamaged case

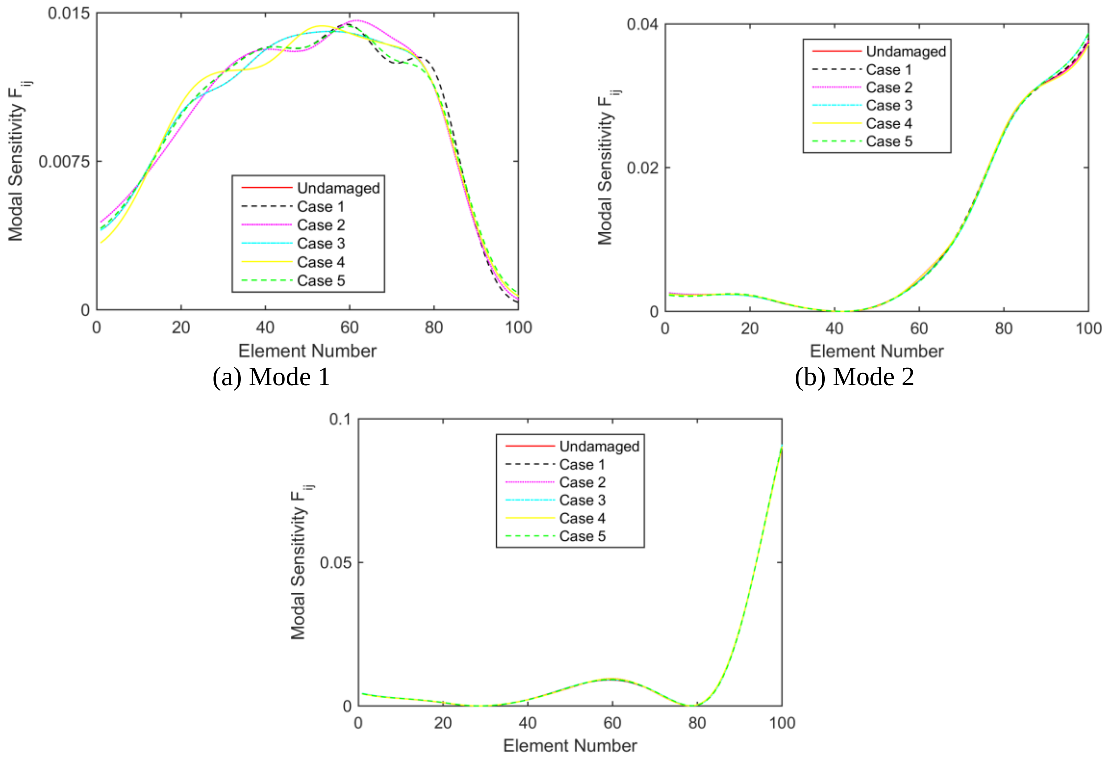

(a) Mode 1 (b) Mode 2

(c) Mode 3

Fig. 10 Comparisons of modal sensitivity before and after damage

Table 4 Damage prediction results of WTT structure using MBDD method

Case	Inflicted Damage Location z (m)	Inflicted Damage DDM element	Predicted Damage Location z (m)	Predicted Damage Range of DDM element	Most Probable Location z (m)	Most Probable DDM element	Location Error (Δz/H) (%)
1	18.7	25	14.2~22.7	19~30	19.6	26	1.17
2	47.7	63	19.6~21.9 & 43.5~48.9	26~29 & 57~64	46.6	61	1.43
3	74.9	98	N/A	N/A	N/A	N/A	N/A
4	18.7, 47.7	25, 63	18.1~22.7, 45~48.1	24~30, 59~63	21.2, 46.6	28, 61	3.25, 1.43
5	18.7, 74.9	25, 98	13.5~20.4, N/A	18~27, N/A	18.1, N/A	24, N/A	0.78, N/A

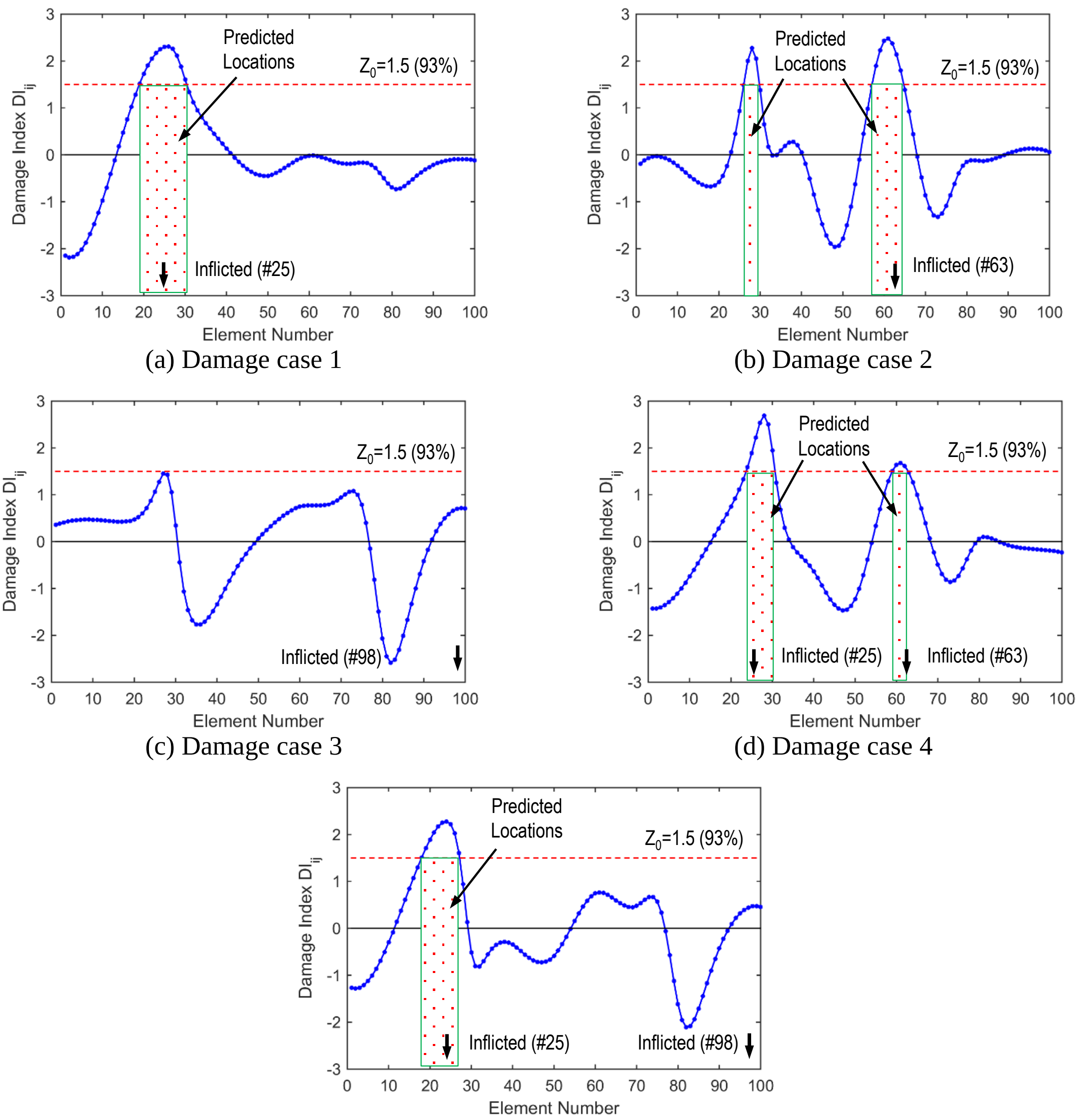

(a) Damage case 1 (b) Damage case 2

(c) Damage case 3 (d) Damage case 4

(e) Damage case 5

Fig. 11 Damage localization results by MBDD method

The accuracy of the damage localization was also evaluated by measuring the localization error le, as listed in Table 4. For single damage cases, it is observed that the localization errors were only 1.17% (0.9 m error) for the damage case 4 and 1.43% (1.1 m error) for the damage case 5. For the multiple damage prediction, the localization errors were 3.25% (2.5 m difference) and 1.43 % (1.1 m difference) for the damage case 4 while the damage case 5 experienced 0.78% (0.6 m difference) and N/A. From all damage cases, damage indices near the element 30 were relatively higher than other locations. It is assumed that the segmental joint simulated near the element might cause somewhat discontinuities in mode shapes and modal curvatures which were utilized for the damage localization.

4. Conclusions

This paper presented two damage detection methods based on the vibration modal parameters to locate damage in wind turbine tower (WTT) structures for which a few frequencies and mode shapes are available. Firstly, a frequency-based damage detection (FBDD) method was outlined. A damage localization algorithm that locates damage from changes in natural frequencies were formulated. Secondly, a mode-shape-based damage detection (MBDD) method was outlined. A damage index algorithm to identify damage from the variations in modal strain energy was formulated. The FBDD method and MBDD method were evaluated for several damage cases simulated on the WTT FE model.

From the numerical studies, it was observed that the FBDD method was very accurate in detecting single damage locations inflicted in the WTT with only three sets of modal parameters. However, the FBDD method was not accurate in detecting multiple damage locations but underestimated in damage localization. By applying the MBDD approach to the WTT, it was observed that damage could be located more accurately in both single and multiple damage cases. However, the MBDD was not accurate in localizing damage simulated near the free-end of the WTT, in which modal sensitivities is relatively low as compared to those of the fixed-end.

Some remaining works are needed for future studies. First, the aerodynamic effect from the rotor system under various wind conditions and the time-varying response of the wind turbine structure due to yawning were not mentioned in this study. Thereby, an appropriate WTT FE model should be established to consider these effects. Secondly, in the normal operation condition, the temperature effect caused by sunlight actually cannot be neglected because modal parameters, especially natural frequency, are quite sensitive with the variation of ambient temperature. Finally, forced vibration tests should be performed on the FE model that the numerically simulated tests are most likely to the field experimental tests.

Acknowledgments

This research was supported by a research grant (Code 12 Technology Innovation E09) from Construction Technology Innovation Program funded by Ministry of Land, Infrastructure and Transport (MOLIT) of Korean government. The graduate students involved in the research were also partially supported by the Brain Korea 21 Plus program of Korean Government.

References

Atkan, A.E., Farhey, D.N., Helmicki, A.J., Brown, D.L., Hunt, V.J., Lee, K.L. and Levi, A. (1997), “Structural identification for condition assessment: experimental arts”, *J. Struct. Eng. - ASCE*, **123**(12), 1674-1684.

Brownjohn, J.M.W., Xia, P.Q., Hao, H. and Xia, Y. (2001), “Civil structure condition assessment by FE model updating: methodology and case studies”, *Finit. Elem. Anal. Des*., **37**(10), 761-775.

Catbas, F.N., Gul, M. and Burkett, J. (2008), “Conceptual damage-sensitive features for structural health monitoring: laboratory and field demonstrations", *Mech. Syst. Signal Pr*., **22**(7), 1650-1669.

Ciang, C.C., Lee, J.R. and Bang, H.J. (2008), "Structural health monitoring for a wind turbine system: a review of damage detection methods", *Meas. Sci. Technol*., **19**(12), 122001-1 -122001-20.

Doebling, S.W., Farrar, C.R. and Prime, M.B. (1998), "A summary review of vibration-based damage identification methods", *J. Shock Vib. Dig*., **30**, 91-105.

Devriendt, C., Weijtjens, W., El-Kafafy, M. and Sitter, B.D. (2014), "Monitoring res resonant frequencies and damping values of an offshore wind turbine in parked conditions", *IET Renewable Power Generation*, 8(4), 433-441.

Dutton, A.G. (2004), "Thermoelastic stress measurement and acoustic emission monitoring in wind turbine blade testing", *Proceedings of the European Wind Energy Conf. EWEC 2004*, London.

Farrar, C.R. and Doebling, S.W. (1997), *An overview of modal-based damage identification methods*, DAMAS 97 (Sheffield, UK).

Ghoshal, A., Sundaresan, M.J., Schulz, M.J. and Pai, P.F. (2000), "Structural health monitoring techniques for wind turbine blades", *J. Wind Eng. Ind. Aerod*., **85**, 309-324.

Gross, E., Simmermacher, T., Rumsey, M. and Zadoks, R.I. (1999), *Application of damage detection techniques using wind turbine modal data*, American Society of Mechanical Engineers Wind Energy Symp. (Reno, NV, USA) AIAA 99-0047.

Hahn, F., Kensche, C.W., Paynter, R.J.H., Dutton, A.G., Kildegaard, C. and Kosgaard, J. (2002), "Design, fatigue test and NDE of a sectional wind turbine rotor blade", *J. Thermoplast. Compos. Mater*., **15**, 267-77.

Jang, S.A., Jo, H., Cho, S., Mechitov, K.A., Rice, J.A., Sim, S.H., Jung, H.J., Yun, C.B., Spencer, Jr., B.F., and Agha, G. (2010), "Structural health monitoring of a cable-stayed bridge using smart sensor technology: deployment and evaluation", *Smart Struct. Syst*., **6**(5-6), 439-459.

Joosse, P.A., Blanch, M.., Dutton, A.G., Kouroussis, D.A., Philippidis, T.P. and Vionis, P.S. (2002), "Acoustic emission monitoring of small wind turbine blades", *Proceedings of the 21st ASME Wind Energy Symp. in conjunction with 40th AIAA Aerospace Sciences Meeting*, Reno, USA, 1–11 & AIAA-2002-0063.

Kim, J.T., Ryu, Y.S., Cho H.M., Stubbs, N. (2003), "Damage identification in beam-type structures: Frequency-based method vs Mode-shape-based method", *Eng. Struct*., **25**, 57-67.

Kim, J.T. and Stubbs, N. (1995), "Model uncertainty and damage detection accuracy in plate-girder bridges", *J. Struct. Eng. - ASCE*, **121**(10), 1409-1417.

Kim, J.T. and Stubbs, N. (2003), "Nondestructive crack detection algorithms for full-scale bridges", *J. Struct. Eng. - ASCE*, **129**(10), 1358-1366.

Kim, J.T., Yun, C.B. and Park, J.H. (2004), "Thermal effects on modal properties and frequency-based damage detection in plate-girder bridges", *Proceedings of SPIE*, **5391**, 400-409.

Lee, J.R. and Tsuda, H. (2005), "A novel fiber Bragg grating acoustic emission sensor head for mechanical tests", *Scr. Mater*., **53**(10), 11811186.

Levin, R.J. and Lieven, N.A.J. (1998), "Dynamic finite element model updating using simulated annealing and genetic algorithms", *Mech. Syst. Signal Pr*., **12**(1), 91-120.

Matsuzaki, R. and Todoroki, A. (2006), "Wireless detection of internal delamination cracks in CFRP laminates using oscillating frequency changes", *Compos. Sci. Technol*., **66**, 407-416.

Perez, I., Cui, H.L. and Udd, E. (2001), "Acoustic emission detection using fiber Bragg gratings", *Proceedings of the SPIE Smart Structures and Materials-Sensory Phenomena and Measurement Instrumentation for Smart Structures and Materials*, USA.

Shi, Z.Y., Law, S.S. and Zhang, L.M. (1998), "Structural damage localization from modal strain energy change", *J. Sound Vib*., **285**(5), 825-844.

Sutherland, H., Beattie, A., Hansche, B., Musial, W., Allread, J., Johnson, J. and Summers, M. (1994), *The application of non-destructive techniques to the testing of a wind turbine blade*, Sandia Report SAND93–1380 Sandia National Laboratories, USA.

Swartz, R.A., Lynch, J.P., Zerbst, S., Sweetman, B. and Rolfes, R. (2009), "Structural monitoring of wind turbines using wireless sensor networks", *Smart Struct. Syst*., **6**(3), 1-14.

Yang, Z., Elgamal, A., Abdoun, T. and Lee, C.J. (2001), "A numerical study of lateral spreading behind a caisson-type quay wall", *Proceedings of the 4th International Conference on Recent Advances in Geotechnical Earthquake Engineering and Soil Dynamics and Symposium*, California, USA, March.

Yun, C.B. and Bahng, E.Y. (2000), "Substructural identification using neural networks", *Comput. Struct*., **77**(1), 41-52.

Yun G.J., Ogorzalek, K.A., Dyke, S.J. and Song, W. (2009), "A two-stage damage detection approach based on subset of damage parameters and genetic algorithms", *Smart Struct. Syst*., **5**(1), 1-21.

Zhang, H., Schulz, M.J., Ferguson, F. and Pai, P.F. (1999), "Structural health monitoring using transmittance functions", *Mech. Syst. Signal Pr*., **13**, 765-787.